Accepted Manuscript

Short-aramid-fiber toughening of epoxy adhesive joint between carbon fiber composites and metal substrates with different surface morphology

Zhi Sun, Shanshan Shi, Xiaozhi Hu, Xu Guo, Jianyun Chen, Haoran Chen

PII: S1359-8368(15)00129-8

DOI: 10.1016/j.compositesb.2015.03.010

Reference: JCOMB 3444

To appear in: *Composites Part B*

Received Date: 18 September 2014

Revised Date: 3 February 2015

Accepted Date: 3 March 2015

Please cite this article as: Sun Z, Shi S, Hu X, Guo X, Chen J, Chen H, Short-aramid-fiber toughening of epoxy adhesive joint between carbon fiber composites and metal substrates with different surface morphology, *Composites Part B* (2015), doi: 10.1016/j.compositesb.2015.03.010.

Short-aramid-fiber toughening of epoxy adhesive joint between carbon fiber composites and metal substrates with different surface morphology

Zhi Sun [1,2,3*], Shanshan Shi [1,2], Xiaozhi Hu [2], Xu Guo [1], Jianyun Chen [3], Haoran Chen [1]

[1] *State Key Laboratory of Structural Analysis for Industrial Equipment, Department of Engineering Mevhanics, Dalian University of Technology, Dalian 116024, China*
[2] *School of Mechanical and Chemical Engineering, University of Western Australia, Perth, WA 6009, Australia;*
[3] *School of Hydraulic Engineering, Dalian University of Technology, Dalian 116024, China*

Abstract: Carbon-fiber epoxy composites were bonded to four different types of aluminum substrates with different surface roughness and finish. The four aluminum substrates considered in this study have the following surface conditions: two solid aluminum substrates polished with two different grades of sandpapers, and two porous aluminum foams with two different as-received surface conditions, one with a patterned surface finish and one with rough pore structures. Moreover, the thin epoxy adhesive joints between the carbon-fiber face sheets and aluminum substrates were reinforced by adding short aramid fibers. During the fabrication process of the hybrid laminar, sparsely-distributed short aramid fibers were inserted between the fiber-metal interface to promote bridged fibers for tougher and stronger adhesive bonding, while at the same time to minimize any significant change in the thickness of the adhesive joint. Measurements of the critical energy release rate showed that the toughening effects of the low-density short aramid fibers were influenced by the metal-substrate surface roughness and finish. Further comparison indicated that the interfacial fracture toughness of aramid-fiber interleave adhesive joints increased via increase of surface roughness of metal substrates. The surface-roughness effect of metal substrate mainly depends on whether the free fiber ends of the short aramid fibers were pressed and embedded into the surface cavities of aluminum substrates according to scanning

[*] Corresponding author. Tel: +86 159 0495 6286; Fax: +86 411 8470 9161;
E-mail addresses: zhisun@dlut.edu.cn (Z. Sun)

electron microscopy observations. The results indicated that the properties and performances of aramid-fiber interleaved adhesive joints between the carbon-fiber face sheets and aluminum substrates could be improved by surface treatments on the aluminum substrates to achieve appropriately surface roughness.

Keywords: A. Aramid fiber; A. Hybrid; B. Adhesion; B. Fracture toughness; Composite adhesive joint

1. Introduction

Carbon-fiber epoxy composites would provide higher specific stiffness, specific strength, fatigue and corrosion resistance than metals, yet, poor impact energy absorption and poor residual strength after impact and delamination [1 – 3]. Therefore, carbon-fiber composites and metal substrates are frequently combined to form hybrid structures for outstanding performance. For instance, fiber metal laminates [1, 4], fiber-metal-foam sandwich [5 – 7] and fiber composites reinforced steel-concrete structures [2, 8] have been explored and developed in aerospace, marine, automotive and civil construction [9 – 16].

For fiber metal hybrid structures consisting of carbon-fiber face sheet on metal substrate, the interface between the face sheet and substrate withstands high in-plane shear stress and out-of-plane stress [17], due to the difference in stiffness between the two different materials and free boundary effects [17]. Meanwhile, interfacial debonding, which may be induced by local contact, low energy impact, accidental excessive loading, or defects during composite processing, are commonly observed in fiber-metal hybrid structures [18]. The high stress level and frequent debonding of fiber-metal interface frequently lead to progressive damage of interface and fatal failure of fiber-metal hybrid structures. Therefore, the global performances of the fiber-metal hybrid structures are often limited by fracture toughness and strength of interface rather than stiffness or strength of fiber composites or metal material. Therefore, the interfacial fracture toughness and toughening method are suggested to be crucial for the fiber-metal hybrid structures, and thus are the focuses of the present study.

Interleave methods [5, 19] are commonly used for fiber/fiber interface to increase the fracture toughness and energy release rate of interfacial adhesive joints. Common interleave materials include nano-tubes, particles, short fibers, thermoplastic and thermoset adhesive films [5, 20 - 25]. Recent study by Yasaee [24, 25] on comparisons between various interleave methods shows that the short aramid fiber interfacial toughening is among the most effective based on both Mode-I and -II fracture toughness measurements of fiber/fiber interface. According to the previous study by Sohn, Walker and Hu [26 - 28], delamination and debonding at fiber/fiber interface were suppressed by microscopic out-of-plane “Z-directional” fiber bridges, which were provided by macroscopic in-plane interleaved short aramid fibers.

However, the interleave methods were not yet fully developed for toughening of adhesive joints between carbon fiber composites and metal substrates, which are becoming increasingly important nowadays, e.g. carbon fiber reinforced/repaired steel structures for building repairing [11] and CARALL [1] for space applications.

Recent study of the authors has showed that the short-aramid-fiber interleave method can also be used to enhance the interfacial fracture toughness between carbon-fiber face sheet and aluminum-foam substrate [5, 6], and between carbon-fiber face sheet and patterned aluminum substrate [29]. Meanwhile, Shi [30] experimentally proved that the short aramid fiber interleave method could prevent interfacial debonding failure of carbon-fiber-aluminum-honeycomb sandwich structures under both bending load and compressive load. However, the parameters of the aramid-fiber interleave, e.g.

fiber density, fiber length and thickness of adhesive joint, in the aforementioned references [5, 6, 29, 30] are different. Moreover, the surface roughness of the metal substrates, i.e. patterned aluminum substrate and aluminum foam, were different. In other words, the surface-roughness effects on the interfacial fracture toughness of interleaved adhesive joints were not yet understood.

One additional potential benefit of understanding the surface-roughness effects is advising surface treatments on metal substrates to create a proper surface roughness for higher interfacial properties. Therefore, a quantitative comparative study on surface-roughness effects of the metal substrate on the fracture toughness of interface with aramid-fiber interleave method is necessary.

The objective of this study is to examine the aramid-fiber interleave methods for adhesive joints of carbon-fiber-metal hybrid structures with metal substrates of various surface roughness. The fracture toughness of plain and aramid-fiber interleaved epoxy adhesive joints between carbon-fiber face sheets and aluminum substrates with four different surface conditions are measured and compared under Asymmetric Double Cantilever Beam (ADCB) condition. The surface-roughness effects of metal substrates on fiber-metal interfaces with aramid-fiber interleaf are examined. In addition, micro scanning electron microscopy (SEM) observations were conducted on the fracture surface to fully understand the toughening mechanism of the aramid-fiber interleaf on fiber metal hybrid structures, and to understand the surface-roughness effect on interfacial fracture toughness.

2. Carbon-fiber aluminum laminates preparation

2.1 Materials

In this study, RC200T/1270 2×2 twill weave (3K) carbon-fiber fabric with an areal density of 200 g/m^2 was used as the face-sheet material. Sandpaper polished 6061 aluminum alloy, Alulight closed-cell aluminum foam with twill-weave surface finish and Alporas closed cell aluminum foam were used as metal substrates to provide surfaces with different conditions and finish. SiC sand papers were chose due to the simplicity in preparation. Another practical reason is that carbon fibers are frequently used to repair metal structures. Surface preparation using sandpaper is convenient for the repairing process, and can be a feasible option.

The short aramid fibers utilized in this study were prepared from Kevlar 49 TM with a diameter of about 12 μm developed by E.I DuPont, while the West System z105 epoxy resin was mixed with slow hardener 206 to create mixed resin. The main properties of the carbon-fiber epoxy face sheet, aluminum substrate and short aramid fibers, adapted from references [28, 31, 32], are listed in Table 1. The surfaces of aluminum substrates are showed in Fig. 1. Surface roughness values, quantified by Ra, of 2400#, 80# sandpaper polished and twill-weave patterned aluminum substrate are 0.29 μm, 0.41 μm and 1.42 μm respectively, measured by Mitutoyo Surftest SJ-210. The surface of Alporas closed cell aluminum foam is distributed with rough pore structures up to 5 mm in diameter and surface roughness measurement is no longer applicable.

2.2 Short aramid fiber preparation

The aramid fiber (Kevlar 49 TM) was initially chopped into 6mm-length, which is the typical length used and recommended in ref [5, 6]. The chopped aramid-fiber strands were next stirred in a blender with blunt blade to produce well-dispersed cotton-like aramid fibers [5]. The cotton-like aramid fibers were then capable to make macroscopically sparsely-distributed thin tissues with desired densities. As an example, the surface view of an aramid-fiber tissue showing the random distributions of short aramid fibers is shown in Fig. 2. The areal density of the short-aramid-fiber tissues used in this study is 12 g/m^2, following refs [5, 6]. In addition, the thin "composite adhesive joints" can effectively prevent a direct contact between the carbon fibers and metal substrates, therefore inhibiting any potential electro-chemical corrosion issue [33] in the hybrid structure.

2.3 Manufacturing of fiber metal laminates

The surfaces of aluminum substrates were firstly degreased using acetone. Then, carbon fiber fabric, aramid-fiber tissue and aluminum substrate were impregnated by epoxy resin. After that, carbon fiber pre-pregs, impregnated aramid-fiber tissue, aluminum-foil pre-crack and aluminum substrate were placed sequentially in mold. The plain specimens were carbon fiber aluminum laminates with pure epoxy adhesive joints (without aramid-fiber tissue). While the toughened specimens were carbon fiber aluminum laminates with aramid-fiber interleaved adhesive joints.

The pre-crack was created by inserting two layers aluminum foil between carbon-fiber face sheet and metal substrate during sample preparation. 10 layers of 0^o carbon fiber fabric were used as face sheet in this study. Two additional layers of carbon-fiber fabric were added to the bottom of Alporas aluminum foam arm to increase the bending stiffness of the bottom arm and provide a smooth surface for assembly of the loading block [5]. Hot press method was used to manufacture the fiber metal laminates [34]. A constant curing pressure of 0.6 MPa was used. And the curing temperature stayed at 110 ^{o}C for half an hour and 140 ^{o}C for another half an hour before cooled down to room temperature as suggested [5, 6].

3. Experimental set-up for interfacial fracture toughness measurement

3.1 Specimen design and dimension

The ADCB geometry [35] was chosen to measure the interfacial fracture toughness quantified as critical energy release rate (G_C) for cracking along the aramid-fiber interleaved interface. Due to the difference in stiffness between the carbon-fiber face sheets and aluminum substrates and the ADCB geometry, G_C measurements are mixed-mode energy release rates. Separations of Mode-I and Mode-II from the mixed-mode energy release rates are also possible, following Ducept [36]. In this study, the following assumptions of continuum mechanics are all valid: 1. The materials have no defects. 2. The properties of all materials remain constant as shown in Table 1. 3. The mass/energy conservation laws are applicable. The validity of the assumptions of continuum mechanics indicates the validity of the mixed-mode measurements of G_C.

Fig. 3 shows a sketch of the ADCB specimen. The total length L and width b of the specimen were 170 mm and 20.0 mm respectively. A pre-crack with 50-mm length and 24-μm thickness was created by inserting two layers of 12-μm-thick aluminum foil between 1.5-mm-thick carbon-fiber face sheet and 15-mm-thick aluminum substrate. Load blocks were bonded to both top and bottom surface.

3.2 Testing condition and evaluation of G_C

Instron 4301 mechanical testing machine was used to conduct the quasi-static ADCB test for measuring the interfacial toughness, quantified as critical energy release rate (G_C). Displacement control mode with a speed of 2 mm/min for both loading and unloading was selected. While the applied load was measured by a 5,000 N load cell.

The ADCB specimens were firstly loaded with the quasi-static rate of 2 mm/min. When the crack extended for 3 – 5 mm, the displacement loading was stopped. Then the specimens were unloaded to zero load to finish a loading-unloading cycle. The loading-unloading cycles were repeated until crack extended to up to 50 mm in this study. The crack extension was measured during the unloading stage, because the interfacial crack would not extend. The crack extension was measured on the side surface of specimen, using an 8×magnification optical travelling microscope with a screw-driven micrometer.

The critical energy release rate G_C, which is the strain energy absorption ability per unit area during crack extension, is calculated as the quotient of energy absorption during interfacial crack extension divided by area of crack extension, as follows:

$$G_c = 1/b \cdot \Delta U / \Delta a \qquad (1)$$

where ΔU is the energy absorption during interfacial crack extension, Δa is the corresponding crack-extension length and b is the width of specimen. The energy absorption during interfacial crack extension was measured using the area under the load-deflection curve minus the strain energy estimated from the unloading curve. The crack tip radius is important for the initial value of G_C, however after crack extension the initial radius has little influence on subsequent measurements. Due to the microscopically uneven surface of metal substrate, the adhesive thickness varies from around 10 to 50 microns. The adhesive thickness variation was due purely to the surface roughness variation. To limit variables, the crack tip radius and average adhesive thickness were kept as 12 and 24 μm in this paper.

4. Experimental results and discussion

4.1 Interfacial fracture toughness

Plain and short-aramid-fiber interleaved specimens with various aluminum substrates were tested using the ADCB methodology described in Section 3. Crack extension up to 50 mm, which is much longer than the length of the interleaved aramid fibers (6 mm), was measured to ensure the fully development of fiber-bridging effect.

The debonding deflected within the interface zone between carbon-fiber face sheet and metal substrate, sometimes within the composite adhesive joint and sometimes along the metal substrate.

A comparison of G_C of adhesive joints without aramid fibers was presented in Table 2. The fact that G_C of brittle epoxy bonded plain specimens in the present study agrees well with previously reported G_C, for example, brittle epoxy bonded aluminum alloy & carbon fiber [37], aluminum & glass fiber [38], epoxy bonded aluminum alloy [39] and toughened epoxy bonded aluminum alloy [35], thus, indicates the validity of the measurements in this study. The primary adhesive concerned in the present study was limited to the common epoxy used for carbon fiber composites so that the surface roughness and its interaction with the composite adhesive joint could be emphasized, which should still be applicable even if tougher adhesives were considered.

The average values and standard deviations of G_C for crack increments from 5 mm to 50 mm of fiber-metal interface are shown in Fig. 4. The average G_C of plain specimens are 105, 174, 27 and 1566 J/m^2 for #2400 sandpaper polished, #80 sandpaper polished, twill-weave patterned and Alporas foam aluminum substrate respectively, while the average G_C of the 6-mm aramid-fiber toughened specimens are 151, 441, 511 and 2720 J/m^2 respectively. The validity of the measurements for the aramid-fiber toughened specimens was verified by comparing with G_C (around 357 – 457 J/m^2) of aramid-fiber toughened epoxy (fiber density 12 g/m^2, fiber length 12 mm, thickness of aramid-fiber toughened zone 24 μm) [29, 40]. It is indicated that G_C of fiber metal laminate with various aluminum substrates have been enhanced due to the low-density short-aramid-fiber interleaf or composite adhesive joints. It is also indicated that the G_C of toughened specimens increase due to the increase in roughness of aluminum substrate.

The G_C values of both plain and toughened specimens show scatters. The scatter was mainly due to the following reasons: (1) different cracking paths, namely crack extensions along the interface between the metal substrate and adhesive joint, or within the plain or interleaved adhesive joint, where bridged fibers may exist, (2) relatively narrow width of specimens (20 mm) in comparison with the aramid-fiber length (6 mm), that aramid-fiber tissue exhibited microscopically uneven distribution. The scatter in adhesive properties appears to be normal if failure can occur along the interface and within the adhesive joint [41]. The scatter can be reduced if a strong bonding between the metal substrate and adhesive joint can be achieved, and if the aramid fiber length is relatively small in comparison to the specimen width, for example, in a real structure.

The different failure modes, underlying toughening mechanism and surface-roughness effect will be discussed in following section in conjunction with SEM observations.

4.2 Fractography and surface-roughness effect

SEM observation on fracture surfaces of specimens was also carried out to fully understand the toughening mechanisms of aramid-fiber interleaved adhesive joints. The fracture surfaces were firstly coated by gold and then examined using a Phillips XL30 SEM at magnifications of 300 times and voltage accelerations of 15kV.

Fig. 5 (a) & (b) respectively showed typical fracture surfaces on the sandpaper-polished substrate bonded with plain epoxy adhesive joint and patterned-surface substrate bonded with interleaved adhesive joint. Back-scattered electrons (BSE) observation in Fig. 5 (a) & (b) showed both the aluminum substrate (bright area) and epoxy resin (dark area) on the fracture surface. The evidence in Fig. 5 confirmed that the two major cracking paths were crack along the metal-substrate surface and crack within the adhesive joints. The fact that both cracks along the metal-substrate surface and within the adhesive joints were observed for plain and toughened specimens suggested that adding aramid fibers could improve the interfacial fracture toughness by toughening and reinforcing the adhesive joints.

In Fig. 5 (b), the fracture surface with fiber pullout marks and residual epoxy indicated a strong interfacial bonding condition. The surface could only be exposed only after peeling off the carbon-fiber face sheet, which suggested that the short aramid fibers created bridges between the carbon-fiber face sheet and metal substrate during crack extension. That is the reason why higher interfacial toughness G_C was performed. Bridged fibers i.e. micro “out-of-plane” short aramid fibers were the primary mechanism for the enhanced energy absorption during crack extension. Moreover, the embedded marks of aramid fibers illustrated that the flexible aramid fibers were pushed onto the small openings of the uneven surface of metal substrate.

It is also evident in Fig. 5 (b) that cracking within the composite adhesive joint with the associated fiber-bridging toughening, and along the interface between the adhesive joint and metal substrate had occurred. The two different failure modes could have contributed to the scatters in G_C measurements shown in Fig. 4, depending on which mode was more dominant during crack extension. Thereby to get effective interlocking aramid-fiber bridges into the surface of a metallic substrate, the undulations/pores generated from surface roughening has to be larger than the diameter of the aramid fibers. Furthermore, the large scatter in Fig. 4 can be reduced by selecting of an adequate fiber density. It should also be mentioned that the toughening mechanism should be applicable to toughened epoxy or other tougher adhesives.

Fig. 6 shows a cross-section view of the composite adhesive joint between the carbon-fiber face sheet and aluminum substrate with patterned surface finish, and sketch on possible toughening mechanisms within plain and interleaved adhesive joint. Fig. 6 (a) indicats that the flexible short aramid fibers can be pressed into the carbon fiber layer and onto the uneven substrate surface, or small cavity if present.

Fig. 6 (b) illustrates three possible cracking paths, i.e. interfacial cracking along the carbon-fiber face sheet, cracking within the adhesive joint, and cracking along the metal substrate. The cracking paths depend on the bonding conditions between the epoxy, carbon fiber and metal materials. In the present study, cracking along the carbon-fiber face sheet was not observed, since the interface between face sheet and adhesive is strong, and the same epoxy is used to make the carbon-fiber face sheet and used as the adhesive. Consequently, cracking within the adhesive joint and along the interface between metal and adhesive joint is emphasized. Fig. 6 (c) thus shows the two major cracking paths of plain epoxy adhesive joint, i.e. within the adhesive joint and along the metal interface. The fracture surface within the adhesive joint and along the metal interface also agreed with the observations in Fig. 5.

Fig. 6 (d) shows flexible short aramid fibers could form micro “out-of-plane” bridges, generated from crack-deflection and crack-branching, particularly relevant to strong interface bonding condition. Even for a thin adhesive joint between 10 to 50 microns, aramid fibers with a diameter of around 12 μm can still be incorporated into the adhesive joint forming a composite adhesive joint as proven in Fig. 6 (a). For a weak bonding/interface between epoxy and metal substrate, the composite adhesive joint may have little effect. However, for a strong bonding condition, crack deflection, crack branching and fiber bridging effects which were created by aramid fibers can significantly enhance the bonding strength and toughness, particularly for a brittle adhesive such as epoxy.

For metal substrate with a relatively smooth surface, the short aramid fibers cannot drop into the surface cavities as the cavities do not exist, or are smaller than the aramid fibers. Thus straight cracking path between the adhesive joint and metal substrate is more likely to occur, other than deflected or branched cracking within composite adhesive joint. Therefore, a rougher metal substrate surface could further enhance the effect of fiber bridging as illustrated in Fig. 6 (d). Indeed, higher G_C values were measured from the laminates with the metal substrate polished with the #80 sandpaper (Ra=0.41 μm), in comparison with the laminates with the substrate polished with the #2400 sandpaper (Ra=0.29 μm).

Fig. 7 shows the in-situ formed “fillet reinforcement” on the aluminum foam substrate, and pullout marks of the composite adhesive joint. The highest G_C of foam laminates could be explained by toughening mechanism of “fillet reinforcement”, where the aramid-fiber toughened epoxy not only adhered to the plate surface but also the vertical walls of open-cell cavities. The presence of short aramid fibers together with resin effectively increased the connecting areas between the carbon-fiber face sheet and the thin wall of aluminum foam, and the in-situ formed fillet reinforcement was strengthened by the short aramid fibers. This fillet-reinforcing mechanism shows that short-aramid-fiber composite adhesive joints with free fiber ends are preferred over continuous-fiber interleaf. The free fiber ends and flexibility of tough and strong aramid fibers are essential for the out-of-plane toughening effects from otherwise in-plane short-aramid-fiber interleaf [23, 29].

5. Conclusion

The effectiveness of the short-aramid-fiber interleaf or composite adhesive joints between carbon-fiber face sheets and aluminum substrates with four different surface conditions have been examined by measuring the corresponding interfacial fracture toughness. Based on the quasi-static ADCB measurements, the composite adhesive joint with interleaved low-density short aramid fibers is able to provide higher fracture toughness than plain adhesive joint, as improvement of varying degree has been observed for all fiber-metal material systems. Specifically, the aramid-fiber interleaf with an areal density of 12 g/m^2 is capable to increase the G_C by around 50 % for all specimens with substrates of different surface characteristics.

Further comparison indicated that the interfacial fracture toughness of aramid-fiber interleave adhesive joints increased via increase of surface roughness of metal substrates. The surface-roughness effect of metal substrate mainly depends on whether the free fiber ends of the short aramid fibers were pressed and embedded into the surface cavities of aluminum substrates according to scanning electron microscopy observations. The aforementioned phenomenon indicates that the fracture toughness of aramid-fiber interleaved adhesive joints could be improved by surface treatments on the aluminum substrates to achieve appropriately surface roughness.

Acknowledgement

The authors are grateful to the financial supports of the Australian Research Council, Australia and the Fundamental Research Funds for the Central Universities. The authors also would like to thank the UWA Centre of Microscopy, Characterization and Analysis for the technical support to the SEM study.

References

[1] Sinmazcelik T, Avcu E, Bora MO and Coban O. A review: Fiber metal laminates, background, bonding types and applied test methods. Materials and Design 2011; 32: 3671-85.
[2] Lau KT, Dutta PK, Zhou LM and Hui D. Mechanics of bonds in an FRP bonded concrete beam. Composites: Part B 2001; 32: 491-502.
[3] Nwosu SN, Hui D and Dutta PK. Dynamic mode II delamination fracture of unidirectional graphite-epoxy composites. Composites: Part B 2003; 34: 303-16.

[4] Botelho EC, Campos AN, Barros ED, Pardini LC and Rezende MC. Damping behavior of continuous fiber/metal composite materials by the free vibration method. Composites: Part B 2006; 37: 255-63.
[5] Sun Z, Jeyaraman J, Sun S, Hu X and Chen H. Carbon-fiber aluminum-foam sandwich with short aramid-fiber interfacial toughening. Composites: Part A 2012; 43: 2059-64.
[6] Sun Z, Hu X, Sun S and Chen H. Energy-absorption enhancement in carbon-fiber aluminum-foam sandwich structures from short aramid-fiber interfacial reinforcement. Composites Science and Technology 2013; 77: 14-21.
[7] Wang L, Liu W-Q, Wan L, Fang H and Hui D. Mechanical performance of foam-filled lattice composite panels in four-point bending: Experimental investigation and analytical modeling. Composites: Part B 2014; 67: 270-9.
[8] Al-Saidy AH, Klaiber FW and Wipf TJ. Strengthening of steel-concrete composite girders using carbon fiber reinforced polymer plates. Construction and Building Materials 2007; 21: 295-302.
[9] Nemat-Nasser S, Kang W-J, McGee JD, Guo W-G and Isaacs JB. Experimental investigation of energy-absorption characteristics of components of sandwich structures. International Journal of Impact Engineering 2007; 34: 1119-46.
[10] Shi S, Sun Z, Ren M, Chen H, Hu X. Buckling response of advanced grid stiffened carbon–fiber composite cylindrical shells with reinforced cutouts. Composites: Part B 2013; 44: 26-33.
[11] Rizkalla S, Dawood M and Schnerch D. Development of a carbon fiber reinforced polymer system for strengthening steel structures. Composites: Part A 2008; 39:388-97.
[12] Lee B-E, Park E-T, Kim J, Kang B-S and Song W-J. Analytical evaluation on uniaxial tensile deformation behavior of fiber metal laminate based on SRPP and its experimental confirmation. Composites: Part B 2014; 67: 154-9.
[13] Guo S-J, Yang Q-S, He XQ and Liew KM. Modeling of interface cracking in copper–graphite composites by MD and CFE method. Composites: Part B 2014; 58: 586-92.
[14] Fiore V, Alagna F, Bella GD and Valenza A. On the mechanical behavior of BFRP to aluminum AA6086 mixed joints. Composites: Part B 2013; 48: 79-87.
[15] Shi S, Sun Z, Ren M, Chen H, Hu X. Buckling resistance of grid-stiffened carbon-fiber thin-shell structures. Composites: Part B 2013; 45: 888-96.
[16] Wang L, Liw W-Q and Hui D. Compression strength of hollow sandwich columns with GFRP skins and a paulownia wood core. Composites: Part B 2014; 60: 495-506.
[17] Benachour A, Benyoucef S, Tounsi A and Adda bedia EA. Interfacial stress analysis of steel beams reinforced with bonded prestressed FRP plate. Engineering Structures 2008; 30: 3305-15.
[18] Marannano GV and Pasta A. An analysis of interface delamination mechanisms in orthotropic and hybrid fiber-metal composite laminates. Engineering Fracture Mechanics 2007; 74: 612-26.
[19] Lee KH, Kim BJ, Yoon SH and Lee DG. Durability improvement of co-cured carbon/epoxy composite-aluminum laminate with nano-size carbon black at cryogenic temperature. Journal of Adhesion Science and Technology 2009; 23: 639-49.
[20] Thakre PR, Lagoudas DC, Riddick JC, et. al. Investigation of the effect of single wall carbon nanotubes on interlaminar fracture toughness of woven carbon fiber–epoxy composites. Journal of Composite Materials 2011; 45: 1091-107.

[21] Hsiao N-M. Compression-after-impact strength and surface morphology in toughened composite materials. International Journal of Fracture 2012; 176: 229-36.

[22] Choi, I., Lee, DG. Surface modification of Carbon Fiber/Epoxy composites with randomly oriented aramid fiber felt for adhesion strength enhancement, Composites: Part A 2013; 48: 1-8.

[23] Hu X-Z and Mai Y-W. Mode I delamination and fiber bridging in carbon-fiber-epoxy composites with and without PVAL coating. Composites Science and Technology 1993; 46: 147-56.

[24] Yasaee M, Bond IP, Trask RS and Greenhalgh ES. Mode I interfacial toughening through discontinuous interleaves for damage suppression and control. Composites: Part A 2012; 43: 198-207.

[25] Yasaee M, Bond IP, Trask RS and Greenhalgh ES. Mode II interfacial toughening through discontinuous interleaves for damage suppression and control. Composites: Part A 2012; 43: 121-128.

[26] Sohn M-S and Hu X-Z. Mode II delamination toughness of carbon-fiber epoxy composites with chopped Kevlar fiber reinforcement. Composites Science and Technology 1994; 52: 439-48.

[27] Sohn M-S, Hu X-Z, Kim J-K and Walker L. Impact damage characterisation of carbon fiber/epoxy composites with multi-layer reinforcement. Composites: Part B 2000; 31: 681-91.

[28] Huang B-Z, Hu X-Z and Liu J. Modelling of inter-laminar toughening from chopped Kevlar fibers. Composites Science and Technology 2004; 64: 2165-75.

[29] Sun Z, Hu X and Chen H. Effects of aramid-fibre toughening on interfacial fracture toughness of epoxy adhesive joint between carbon-fibre face sheet and aluminium substrate. International Journal of Adhesion and Adjesives 2014; 48: 288-94.

[30] Shi, S, Sun, Z, Hu, X, Chen, H, Carbon-fiber and aluminum-honeycomb sandwich composites with and without Kevlar-fiber interfacial toughening, Composites: Part A 2014; 67: 102-10.

[31] Rattan R, Bijwe J and Fahim M. Influence of weave of carbon fabric on low amplitude oscillating wear performance of Polyetherimide composites. Wear 2007; 262: 727-35.

[32] Idris MI. Structural integrity of carbon fiber/aluminium foam sandwich composites [D]. Degree of Doctor of Philosophy in Materials Science and Engineering, The University of New South Wales 2010.

[33] Lin C-T and Kao P-W. Delamination growth and its effect on crack propagation in carbon fiber reinforced aluminum laminates under fatigue loading. Acta Materialia 1996; 44: 1181-8.

[34] Sinmazçelik T, Avcu E, Bora MÖ and Çoban O. A review: Fibre metal laminates, background, bonding types and applied test methods. Materials and Design 2011; 32: 3671-85.

[35] Datla NV, Papini M, Ulicny J, Carlson B and Spelt JK. The effects of test temperature and humidity on the mixed-mode fatigue behavior of a toughened adhesive aluminum joint. Engineering Fracture Mechanics 2011; 78: 1125-39.

[36] Ducept F, Gamby D and Davies P. A mixed-mode failure criterion derived from tests on symmetric and asymmetric specimens. Composites Science and Technology 1999; 59: 609-19.

[37] Zhu G-Z, Zheng C-L and Lu X-F. The influence of loading rate on the interfacial fracture toughness of carbon fiber-metal laminates based on magnesium alloy.

Advanced Materials Research 2011; 328-330: 1373-76.

[38] Cao HC and Evans AG. An experimental study of the fracture resistance of bimaterial interfaces. Mechanics of Materials 1989; 7: 295-304.

[39] Bouchet J, Roche AA and Jacquelin E. The role of the polymer/metal interphase and its residual stresses in the critical strain energy release rate (G_C) determined using a three-point flexure test. Journal of Adhesion Science and Technology 2001; 15: 345-69.

[40] Andrews EH and Stevenson A. Fracture energy of epoxy resin under plane strain conditions. Journal of Materials Science 1978; 13: 1680-8

[41] Saleema N, Sarkar DK, Paynter RW, et al. A simple surface treatment and characterization of AA 6061 aluminum alloy surface for adhesive bonding applications. Applied Surface Science 2012; 261: 742-48.

Figure and Table Captions

Fig. 1. Different surface conditions of aluminum substrates; (a) 2400# sandpaper polished surface, (b) 80# sandpaper polished surface, (c) patterned surface comparable to carbon fiber cloth, (d) rough aluminum-foam surface with pores up to 5 mm in diameter.

Fig. 2. Surface view of distributed short aramid-fiber tissue (fiber length: 12 mm).

Fig. 3. Schematic of Asymmetric Double Cantilever Beam (ADCB) specimen.

Fig. 4. Average critical energy release rate of plain and toughened sandwich specimens (error bars showing the standard deviation, and the large scatter for interface-toughened composites can be at least partially due to the difference in cracking path, i.e. along metal substrate or within the adhesive joint).

Fig. 5. Fracture surface on aluminum substrate after peeling off the face sheet; (a) plain specimen with 80# sandpaper surface finish, (b) fiber-toughened specimen with the patterned surface finish, the two dotted circles showing the pullout marks of bridging aramid fibers (one with free fiber end) originally embedded in surface cavities.

Fig. 6. (a) short aramid-fiber toughened adhesive joint around 20-μm-thick (the adhesive thickness varies at different locations due to surface roughness), (b) sketch of three possible cracking paths within adhesive joint, (c) sketch of adhesive joint without aramid fibers, and two possible failure patterns, (d) sketch of adhesive joint with reinforcing aramid fibers. Free fiber ends of flexible aramid fibers can be pressed into the above carbon fiber ply and pressed down to the uneven metal substrate. Such “misalignment” will be reduced for a thinner adhesive joint.

Fig. 7. In-situ formed “filler reinforcement” on the aluminum foam surface; (a) cross-section view, (b) sketch of the composite adhesive joint between carbon-fiber face sheet and aluminum foam substrate [6] and viewing direction of SEM observations, (c) fracture feature close to a thin aluminum wall between pores, showing the composite adhesive joint and pullout section.

Table 1. Properties of the carbon-fiber epoxy face sheet, short aramid fibers and aluminum substrates.

Table 2. Comparison of G_C of epoxy adhesive joints

Table 1. Properties of the carbon-fiber epoxy face sheet, short aramid fibers and aluminum substrates.

Properties (Symbol) [units]	Carbon fiber/epoxy	Aramid fiber	6061 aluminum alloy	Alulight aluminum foam	Alporas aluminum foam
Density [kg/m^3]	1530	1400	2800	300-1000	200-250
Young's Modulus [GPa]	106	131	69	1.7-12	0.4-1.0
Comp. Strength [MPa]	-	-	-	1.9-14	1.3-1.7
Tensile strength [MPa]	888	2655	462	2.2-30	1.6-1.9
Poisson's Ratio (ν/ν_{12})	0.3	0.3	0.3	0.31-0.34	0.31-0.34

Table 2. Comparison of G_C of epoxy adhesive joints

Resource	Materials system	G_C (J/m^2)
Ref. 37	Magnesium-aluminum alloy & carbon fiber/epoxy	0.5 ~ 2
Ref. 38	Aluminum alloy & glass fiber/epoxy	6 ~ 25
This study	Patterned Aluminum & carbon fiber/epoxy	10 ~ 40
Ref. 39	Degreased aluminum & epoxy	20~ 66
This study	Sandpaper polished Aluminum & carbon fiber/epoxy	50 ~ 200
Ref. 35	Aluminum alloy & toughened epoxy	100 ~ 200

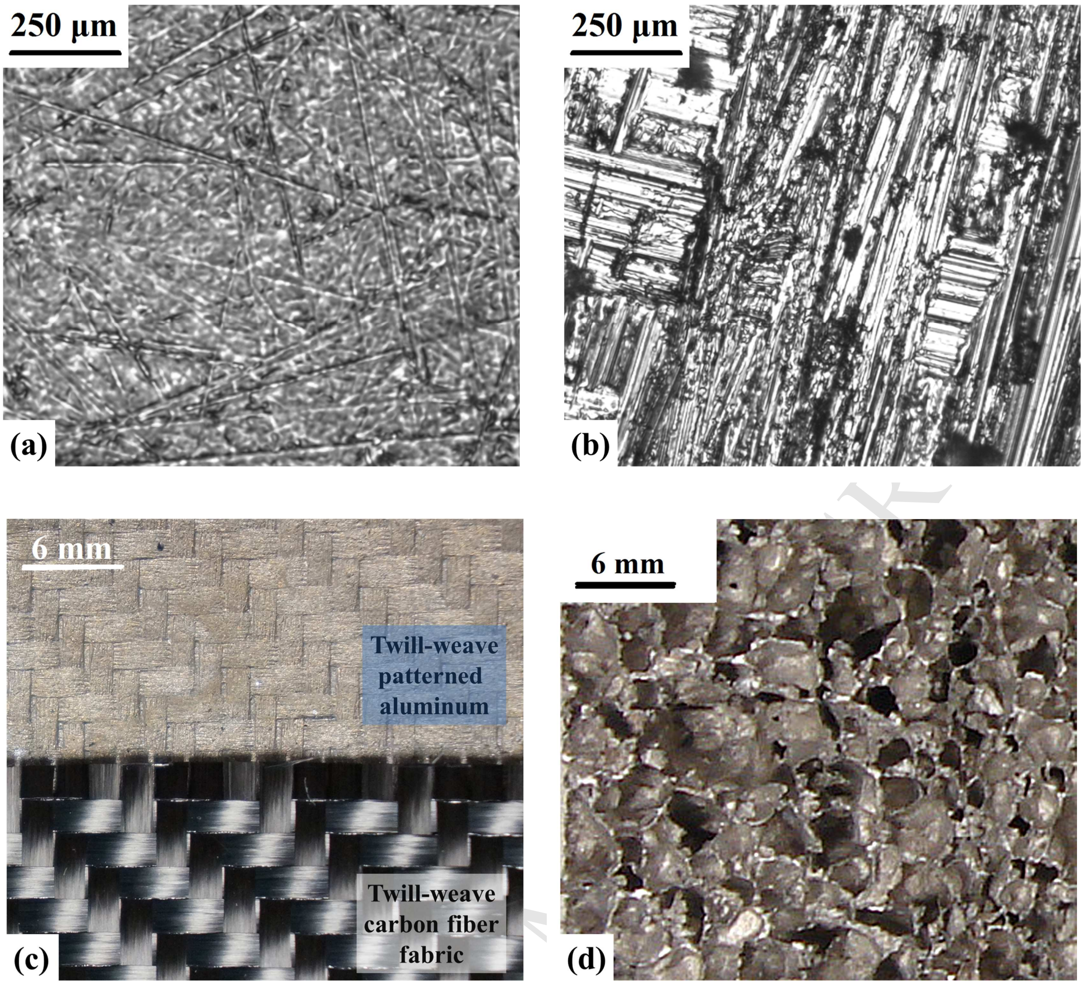

Fig. 1. Different surface conditions of aluminum substrates; (a) 2400# sandpaper polished surface, (b) 80# sandpaper polished surface, (c) patterned surface comparable to carbon fiber cloth, (d) rough aluminum-foam surface with pores up to 5 mm in diameter.

Fig. 2. Surface view of distributed short aramid-fiber tissue (fiber length: 12 mm)

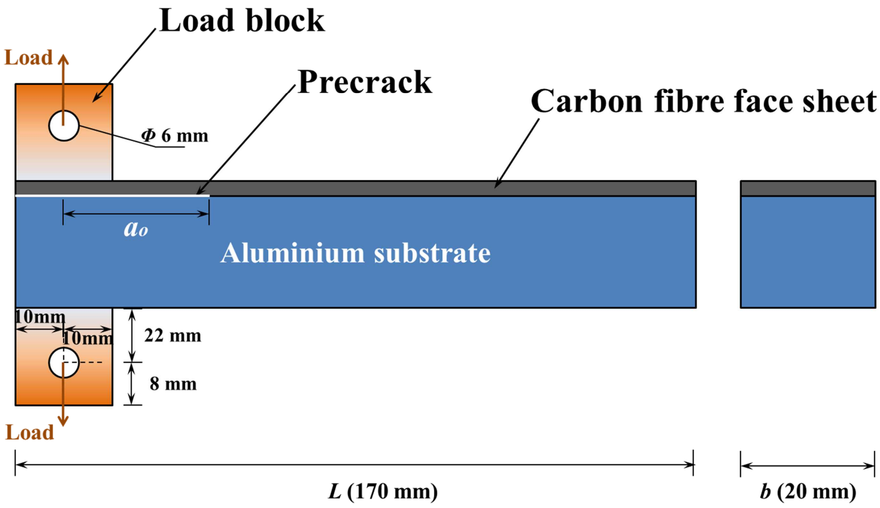

Fig. 3. Schematic of Asymmetric Double Cantilever Beam (ADCB) specimen

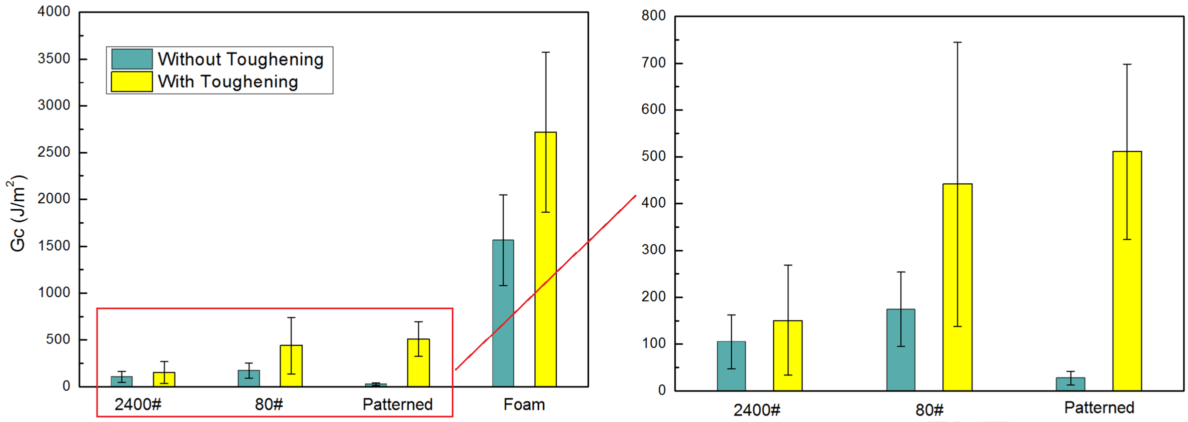

Fig. 4. Average critical energy release rate of plain and toughened sandwich specimens (error bars showing the standard deviation, and the large scatter for interface-toughened composites can be at least partially due to the difference in cracking path, i.e. along metal substrate or within the adhesive joint).

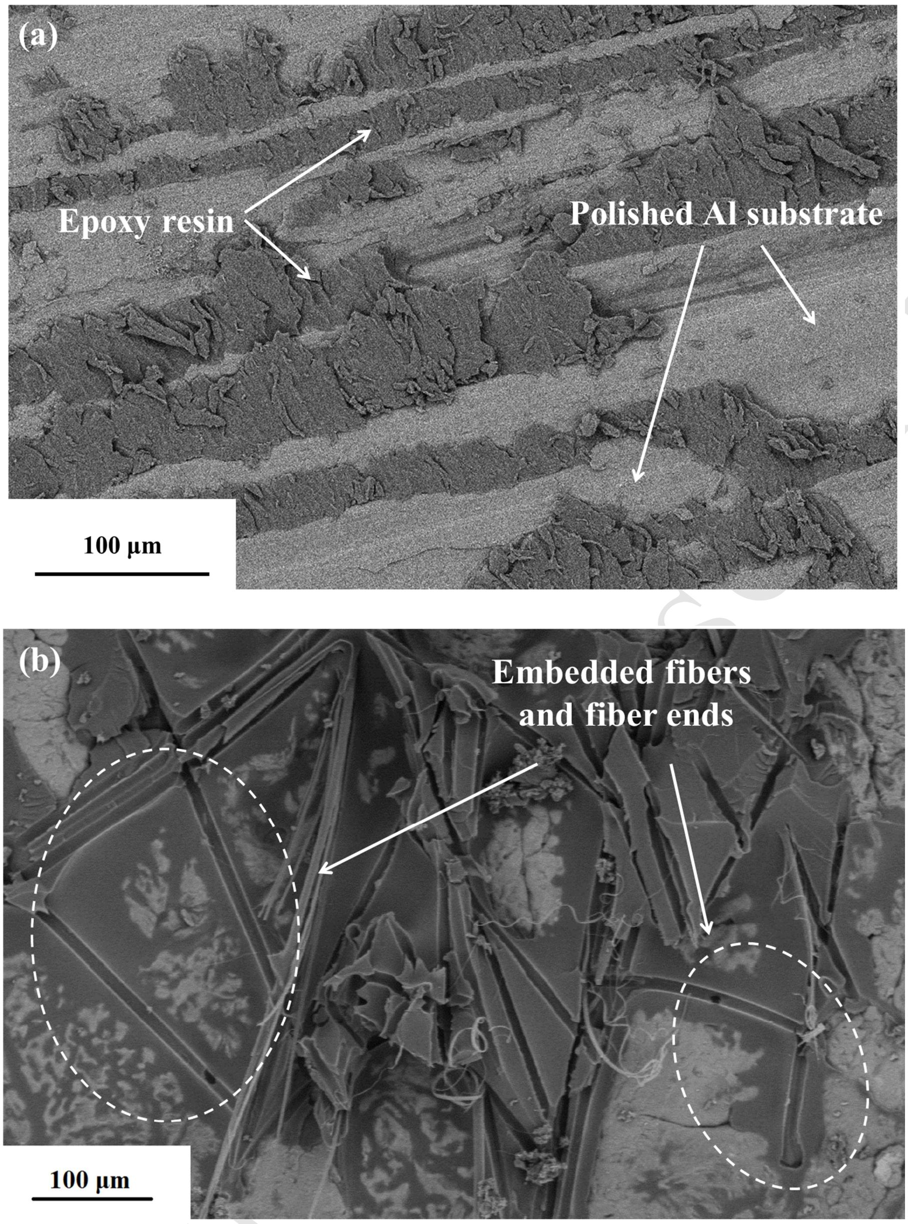

Fig. 5. Fracture surface on aluminum substrate after peeling off the face sheet; (a) plain specimen with 80# sandpaper surface finish, (b) fiber-toughened specimen with the patterned surface finish, the two dotted circles showing the pullout marks of bridging aramid fibers (one with free fiber end) originally embedded in surface cavities.

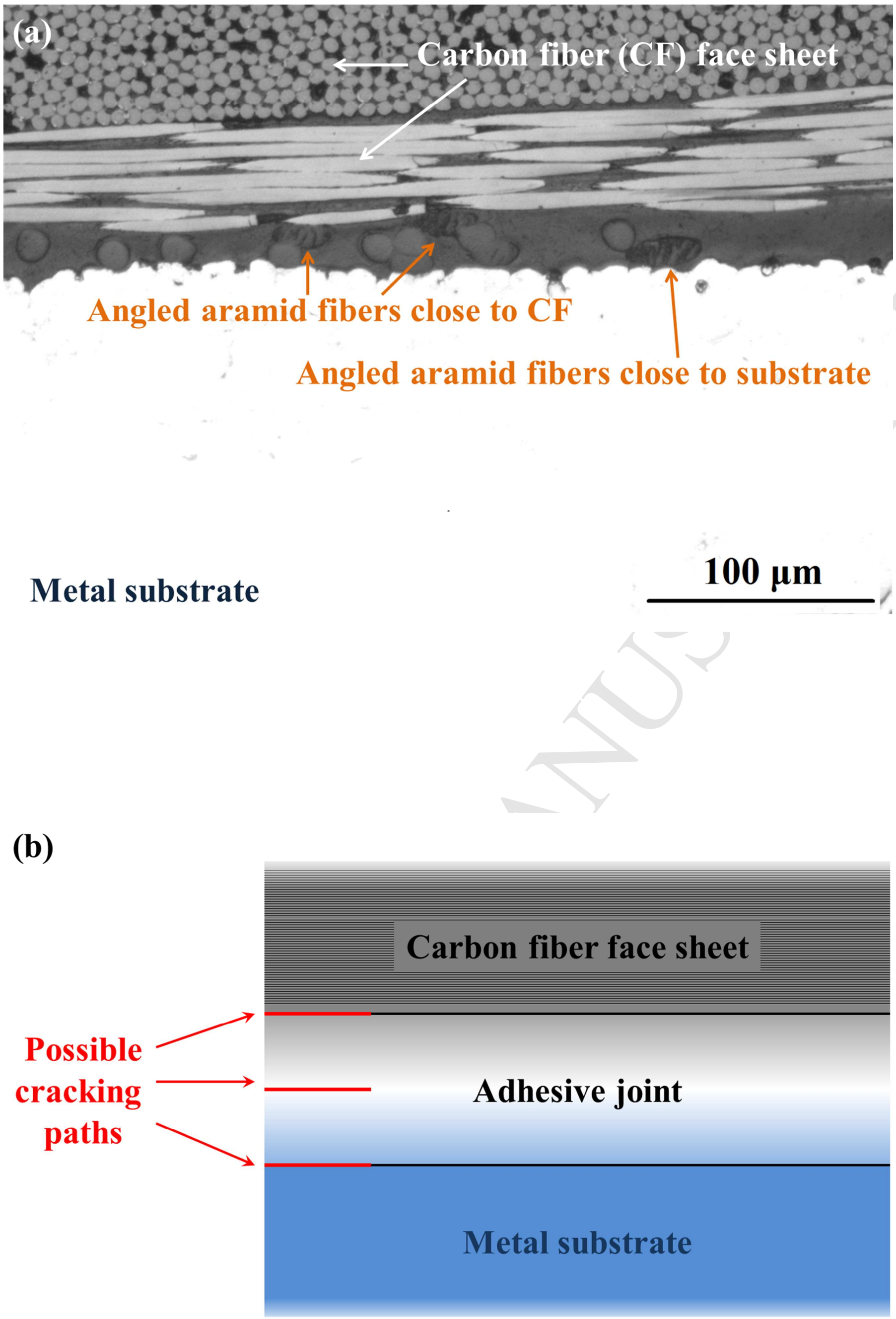
(a)
Carbon fiber (CF) face sheet
Angled aramid fibers close to CF
Angled aramid fibers close to substrate
Metal substrate
100 µm
(b)
Carbon fiber face sheet
Possible
cracking
paths
Adhesive joint
Metal substrate

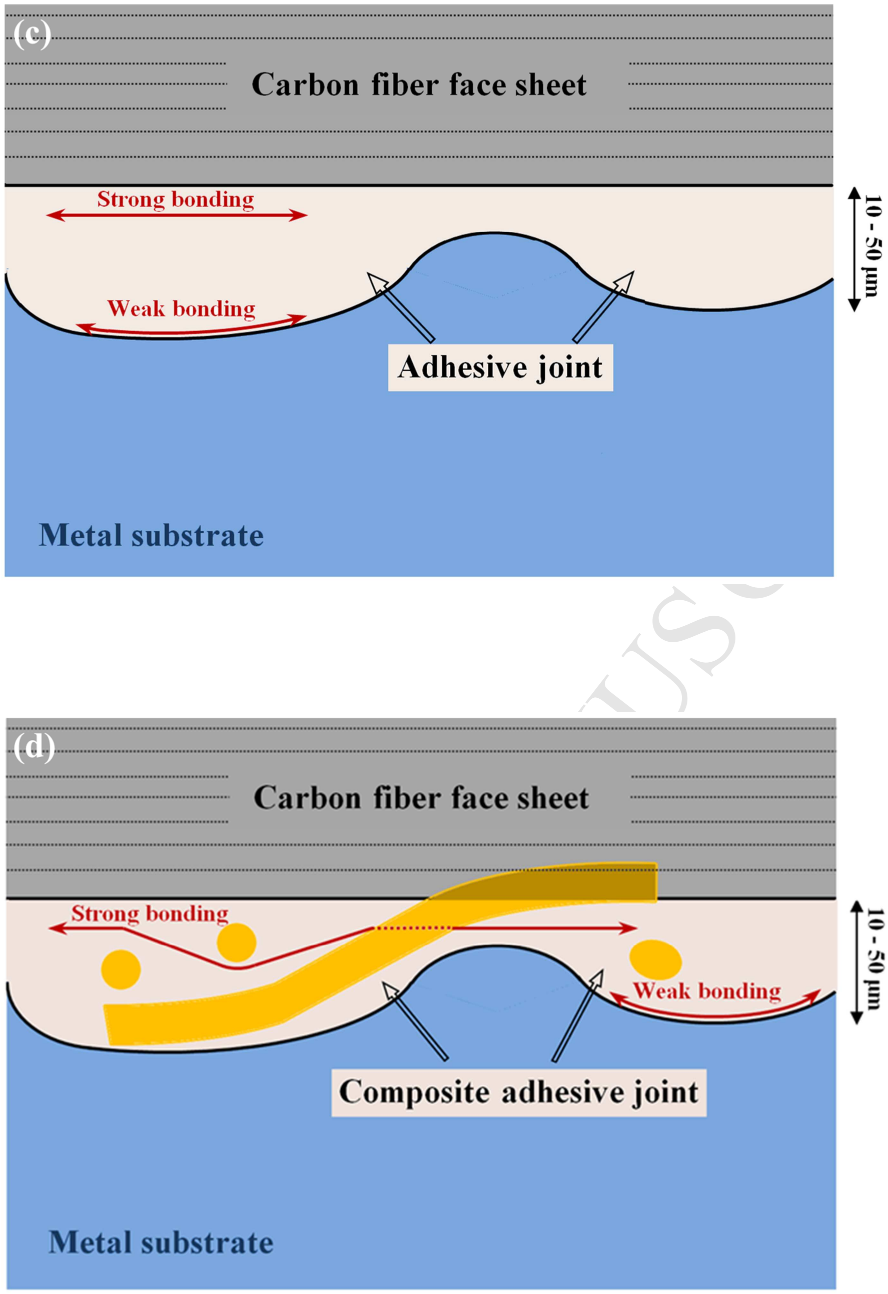

Fig. 6. (a) short aramid-fiber toughened adhesive joint around 20-μm-thick (the adhesive thickness varies at different locations due to surface roughness), (b) sketch of three possible cracking paths within adhesive joint, (c) sketch of adhesive joint without aramid fibers, and two possible failure patterns, (d) sketch of adhesive joint with reinforcing aramid fibers. Free fiber ends of flexible aramid fibers can be pressed into the above carbon fiber ply and pressed down to the uneven metal substrate. Such “misalignment” will be reduced for a thinner adhesive joint.

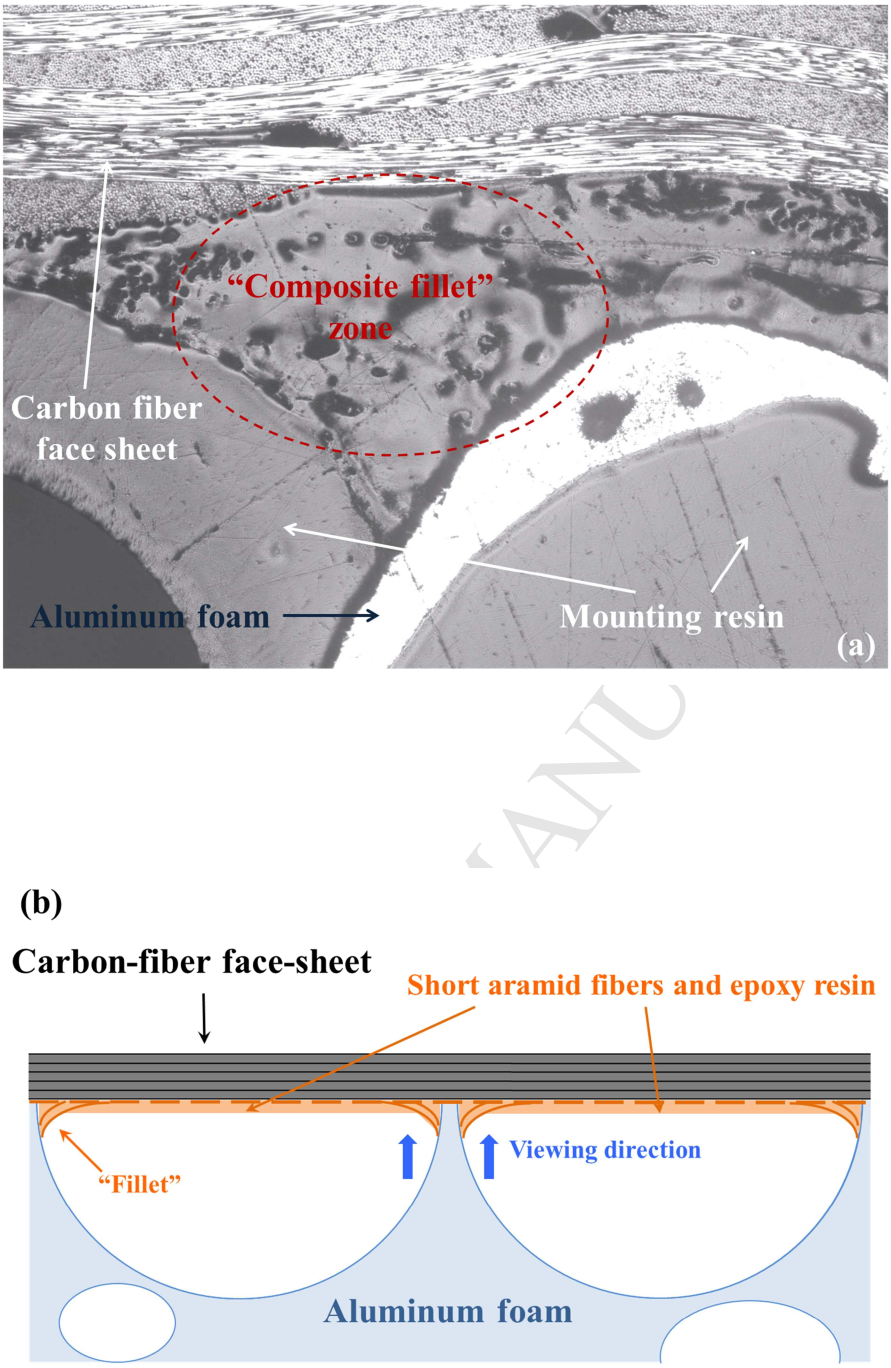

"Composite fillet" zone
Carbon fiber face sheet
Aluminum foam
Mounting resin
(a)
(b)
Carbon-fiber face-sheet
Short aramid fibers and epoxy resin
"Fillet"
Viewing direction
Aluminum foam

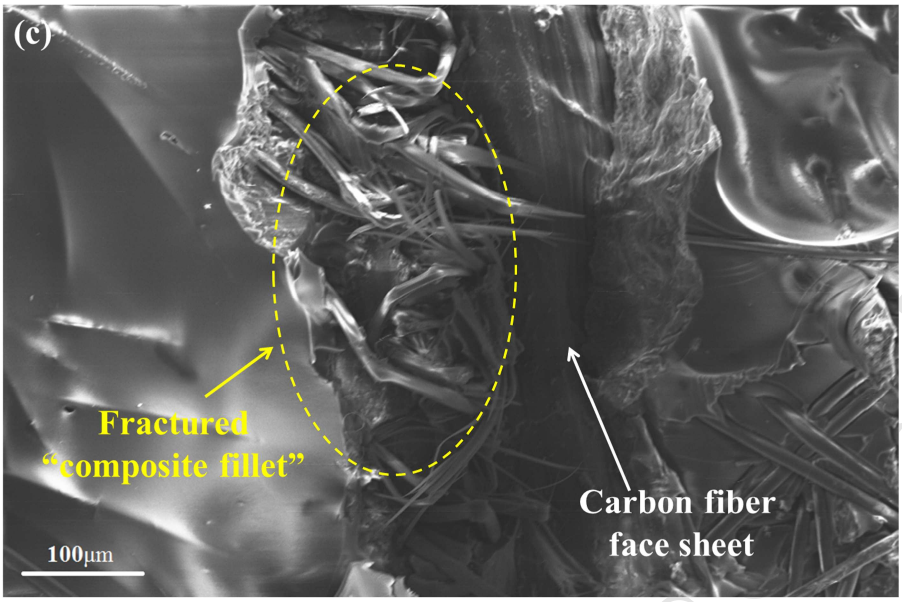

Fig. 7. In-situ formed "filler reinforcement" on the aluminum foam surface; (a) cross-section view, (b) sketch of the composite adhesive joint between carbon-fiber face sheet and aluminum foam substrate [6] and viewing direction of SEM observations, (c) fracture feature close to a thin aluminum wall between pores, showing the composite adhesive joint and pullout section.